Journal of Catalysis **204,** 238–248 (2001)
doi:10.1006/jcat.2001.3379, available online at http://www.idealibrary.com on IDEAL®

Effect of Thermal Sintering on Light-Off Performance of Pd/(Ce,Zr)O_x/Al_2O_3 Three-Way Catalysts: Model Gas and Engine Tests

A. Martínez-Arias,*,[1] M. Fernández-García,* A. B. Hungría,* A. Iglesias-Juez,* K. Duncan,† R. Smith,† J. A. Anderson,‡ J. C. Conesa,* and J. Soria*

*Instituto de Catálisis y Petroleoquímica, CSIC, Campus Cantoblanco, 28049 Madrid, Spain; †Department of Electronic Engineering and Physics, University of Dundee, Dundee, Scotland, United Kingdom; and ‡Department of Chemistry, University of Dundee, Dundee, Scotland, United Kingdom

Received June 7, 2001; revised July 31, 2001; accepted July 31, 2001

The effect of thermal degradation on the catalytic performance in light-off tests of Pd three-way catalysts supported on alumina and promoted with Ce–Zr mixed oxides has been investigated either under synthetic gas mixtures (for catalysts in powder form) or in engine tests (for catalyst monoliths). Accelerated aging of the systems by oven heating at 1273 K produces a significant sintering of both Pd and Ce–Zr mixed oxide active components, indicated by X-ray diffraction, transmission electron microscopy, and diffuse reflectance Fourier transform infrared (DRIFTS) techniques. In spite of these effects, the small differences between the light-off performances of fresh and aged systems show the relatively low relevance (particularly in real conditions under engine emissions) of the thermal degradation on the overall performance of the system. *In situ* **DRIFTS results suggest that this is the result of the relatively low structural sensitivity of the desorption of hydrocarbon fragments adsorbed on the active sites, which act mainly as self-poisons for the catalytic reactions.**

Key Words: **Pd three-way catalysts; Ce–Zr mixed oxides; ceria; zirconia; alumina; monolith; XRD; TEM–EDS;** *in situ* **DRIFTS.**

I. INTRODUCTION

Three-way catalysts (TWC) have been widely used to simultaneously reduce emissions of hydrocarbons (HC), CO, and nitrogen oxides (NO_x) from gasoline engine powered vehicles (1). Classical components of these systems usually include Rh, Pt, and/or Pd as active metals, and ceria as promoter (1, 2). More recently, the use of Pd as the only active metal component in TWC has received considerable attention on the basis of economical aspects (the high cost and scarcity of Rh) and the availability of cleaner fuels, and despite limitations for NO_x reduction reactions (3–6), this component exhibits a remarkable activity for HC and CO oxidation reactions. On the other hand, the classical promotion by ceria has been extended to other oxide systems aiming to increase or maintain the durability of the TWC while decreasing the toxic emissions produced during the cold-start (or light-off) period, which may represent a considerable portion of the whole emissions produced during any driving cycle (1, 7). Among these latter, Ce–Zr mixed oxide systems have been proposed as potential replacements for ceria on the basis of their larger oxygen-storage capacity (OSC) after thermal sintering, which would eventually help to decrease the cold-start emissions mainly by permitting the catalyst to be located in positions closer to the engine, with lower system deactivation being produced (8).

A degree of controversy exists in respect to the optimum configuration (Al_2O_3-supported or unsupported) of Ce–Zr components in these catalysts. Jiang *et al.* (9) propose employment of unsupported materials based mainly on the more precise control at a compositional–morphological level, for achievement of optimal catalytic properties, which could potentially be achieved, and on assuring establishment of interactions between noble metals and the mixed oxide component (9). However, recent investigations have shown the superior redox properties of the alumina-dispersed nanoparticle mixed oxide configurations, in comparison with unsupported cases (at least when treatments leading to surface–textural modifications have not been performed (10)), in terms of the dynamic-OSC achieved, particularly for systems aged under air at 1273–1373 K (11). Additionally, recent catalytic activity results under stoichiometric CO–NO–O_2 reactant mixtures suggest the involvement of Pd interaction with Al_2O_3-dispersed mixed oxide entities as the active sites for NO reduction reactions (12). Nevertheless, important difficulties must be considered in the preparation of alumina-supported mixed oxide in its most active phases, which involve Ce/Zr atomic ratios close to or slightly higher than one (11, 13). Promising results in this respect have been obtained by employing a reverse microemulsion approach, as structurally homogeneous

[1] To whom correspondence should be addressed. E-mail: amartinez@icp.csic.es. Fax: 34 91 5854760.

0021-9517/01 $35.00

nanoparticle configurations of the mixed oxide are achieved as a consequence of the spatial confinement to which the precursors are subjected within the microemulsion (14, 15).

In this context, it is desirable to determine which are the main parameters affecting light-off performance for this kind of materials. With this objective in mind, a catalyst in which ceria–zirconia promoters have been incorporated by the microemulsion method onto an alumina precoated monolith has been tested with regard to its catalytic performance under light-off conditions, employing the exhaust gas produced by a gasoline engine as reactant. In order to examine the influence of thermal degradation on the catalytic properties of the system, two different initial conditions, fresh and oven-aged at 1273 K (as a benchmark temperature at which loss of structural homogeneity is produced in the Ce–Zr mixed oxide (11, 13)), were employed. The results are compared with those observed for powdered catalysts prepared using the same method and examined under stoichiometric synthetic gas mixtures by catalytic activity tests in a laboratory reactor, characterising the processes occurring during the catalytic reactions by *in situ* diffuse reflectance Fourier transform (DRIFTS). X-ray diffraction (XRD) and transmission electron microscopy–energy dispersive X-ray spectroscopy (TEM–EDS) techniques are employed to characterise the catalysts.

II. EXPERIMENTAL

A. Catalyst Preparation

Cordierite monoliths (kindly supplied by Johnson Matthey, 152-mm length, 101-mm diameter) with 400 cells per square inch were used as support. These were coated with alumina by employing a dip-coating procedure using colloidal solutions prepared by dissolving 200 g of boehmite powder Disperal SOL P-3 (from Condea) in 1.5 l of water acidified with 10 ml of concentrated HNO_3 (Panreac, 60 w/v%); an initial pH of ca. 1.0, which increased to ca. 4.0 on introduction of the boehmite, was observed in these conditions. The preparation was followed by drying and calcination in air at 1073 K for 2 h. About 130 g of alumina was incorporated into the monolith on the basis of weight difference. The ceria–zirconia promoter was deposited on the alumina-coated monolith by employing reverse microemulsions of similar characteristics (in terms of the constituent nature and volumes employed) as those described in previous articles (14, 16). The procedure consisted of successive immersions of the monolith, first into a microemulsion (with *n*-heptane as organic phase, Triton X-100—from Aldrich—as surfactant, and hexanol as cosurfactant) containing the cerium–zirconium precursors (cerium(III) nitrate and zirconyl nitrate, Alfa Aesar) in its aqueous phase in an amount chosen to give a maximum 15 wt% CeO_2–ZrO_2 in the washcoat and then, after blowing off the unretained liquid, into a second microemulsion of similar characteristics containing the base (tetramethylammonium hydroxide (Alfa Aesar)) in its aqueous phase. Subsequently, the monolith containing the coprecipitated cerium and zirconium precursors was dried for 24 h at 393 K and calcined in air at 773 K for 2 h. Finally, palladium was applied on the monoliths by direct impregnation, filling the monolith channels with Pd(II) nitrate (from Alfa Aesar) aqueous solution, followed by drying at 393 K for 24 h and calcination in air at 773 K for 2 h. This sample will be hereafter referred to as fresh PCZ-m. Oven aging of the catalysts was carried out under air at 1273 K for 16 h. The main characteristics of the washcoat in these catalysts were as follows: according to chemical analysis measurements (performed by ICP–AES at the Centro de Espectrometría Atómica, UCM), the weight percent values of Pd, CeO_2, and ZrO_2 were 0.77, 3.69 and 2.01, respectively (corresponding to 0.83, 4.00, and 2.18 g per l of monolith geometric volume, respectively). This corresponds to a Ce/Zr atomic ratio of 1.31. In turn, S_{BET} values for the wash coat in fresh and aged PCZ-m were 184 and 87 $m^2\,g^{-1}$, respectively. A commercial Pt–Rh monolithic TWC (supplied by Johnson Matthey) has been used as a reference for the engine tests.

A reference powder catalyst containing 1 wt% Pd and 10 wt% $CeZrO_4$ promoter (compositions confirmed by ICP–AES chemical analysis) on alumina (Condea Puralox, $S_{BET} = 180\,m^2\,g^{-1}$) was prepared by employing methods and precursors similar to those used for preparation of the catalyst monoliths. Full details of the procedure employed can be found elsewhere (14, 15). This will be referred to as fresh PCZ-p while the 10 wt% $CeZrO_4$ supported on alumina employed in this preparation will be referred to as CZ. The aging procedure was in every case similar to that employed for the catalyst monoliths. S_{BET} values obtained for the fresh and aged PCZ-p catalyst were 194 and 85 $m^2\,g^{-1}$, respectively.

B. Engine Testing

Light-off tests from ambient temperature were performed with a gasoline-fuelled spark ignition 1.8-l Volkswagen engine (model year 1990, electronic spark ignition and fuel injection with Bosch K Jetronic carburettion) with four cylinders and fitted with an oxygen sensor for λ control, using commercial lead-free gasoline (BP 95 RON, specification number BSEN 228; 100 ppm S according to commercial specification) as fuel. Operation conditions were maintained constant during the tests at ca. 1600 rpm rotational speed and ca. 6.0 N m torque, under slope conditions (corresponding to an estimated space velocity of ca. 24,000 Nl $l^{-1}\,h^{-1}$). Two different tests were run consecutively under those conditions, the first beginning from ambient temperature with the start of the engine; then, the exhaust temperature was increased under the above-mentioned conditions

until a stationary condition was achieved (cold-start test). Subsequently, the engine was stopped, and a second test was performed by restarting the engine after the exhaust temperature had decreased to about 473 K, again allowing the system to reach its stationary condition under the above-mentioned conditions (hot-start test). As similar activity vs temperature profiles were obtained in both tests, only results of the cold-start test are presented. The aftertreatment system consisted of a single catalyst located ca. 1 m from the engine manifold, simulating the under-floor position of an actual vehicle. Temperature monitoring was performed using two thermocouples located ca. 1 cm before and after the catalyst. Analysis of the emitted gases was achieved with a signal detection system consisting of a FID (flame ionization detector) analyser for total hydrocarbon (THC) concentration measurements (concentrations being referred to propane, which is employed as reference gas for calibration), infrared detectors for CO and CO_2 concentrations, a paramagnetic analyser for O_2 concentration, and a chemiluminiscence analyser for NO_x ($NO + NO_2$) analysis.

C. Laboratory Reactor Tests on Powdered Catalysts

Catalytic tests using a model gas stoichiometric mixture of 1% $CO + 0.1\%$ $C_3H_6 + 0.1\%$ $NO + 0.9\%$ O_2 (N_2 balance) at 30,000 h^{-1} were performed in a Pyrex glass reactor system. Reference tests ($CO–O_2$ and $CO–O_2–NO$ reactions) under stoichiometric conditions were carried out with the same system by using 1% $CO + 0.5\%$ O_2 and 1% $CO + 0.45\%$ $O_2 + 0.1\%$ NO (N_2 balance) mixtures at 30,000 h^{-1}(all concentrations in volume percent units). After grinding and sieving, catalyst particles in the 0.12- to 0.25-mm range, for which internal diffusion effects were minimised (15), were employed for these tests. Gases were regulated with mass flow controllers and analysed using an on-line Perkin–Elmer 1725X Fourier transform infrared (FTIR) spectrometer coupled with a multiple reflection transmission cell (Infrared Analysis Inc.). Oxygen concentrations were determined using a paramagnetic analyser (Servomex 540A). Prior to catalytic testing, *in situ* calcination was performed using synthetic air at 773 K, followed by cooling in synthetic air and a N_2 purge at room temperature (RT). A standard test consisted of increasing the temperature from 298 to 823 K at 5 K min^{-1}.

D. Characterisation Techniques

DRIFTS analysis of adsorbed species present on the catalyst surface under reaction conditions was carried out using a Perkin–Elmer 1750 FTIR fitted with a mercury cadmium telluride detector. Analysis of the NO conversion at the outlet of the IR cell was performed by chemiluminescence (Thermo Environmental Instruments 42C). The DRIFTS cell (Harrick) was fitted with CaF_2 windows and a heating cartridge that allowed samples to be heated to 773 K. Samples of ca. 65 mg were calcined *in situ* (in a similar manner as employed for the laboratory reactor tests) and then cooled to 298 K in synthetic air before introducing the reaction mixture and heating at 5 K min^{-1} up to 673 K, recording one spectrum (4-cm^{-1} resolution, average of 100 scans) generally every 15 K. The gas mixture (similar to that employed for laboratory reactor tests) was prepared using a computer controlled gas blender with 60 cm^3 min^{-1} passing through the catalyst bed.

TEM experiments were carried out using a JEOL 2000 FX (0.31-nm point resolution) equipped with a LINK (AN 10000) probe for EDS analysis. The sample spot for EDS analysis is in the 50 to 100-nm range. Portions of samples were crushed in an agate mortar and suspended in butyl alcohol. After ultrasonic dispersion, a droplet was deposited on a copper grid supporting a perforated carbon film. Micrographs, electron diffractograms, and, where necessary, dark-field images were recorded over selected areas, with compositions previously characterised by EDS. Between 6 and 10 aggregates of a typical size of 200–300 nm were studied for each sample, analysing about two to four different zones of each aggregate. by TEM–EDS.

Powder XRD patterns were recorded on a Siemens D-500 diffractometer using nickel-filtered CuKα radiation operating at 40 kV and 25 mA and with a 0.025° step size.

III. RESULTS AND DISCUSSION

A. Structural Properties

Powder X-ray diffractograms of fresh and aged PCZ-p and PCZ-m catalysts are shown in Fig. 1. Peaks arising from the Ce–Zr mixed oxide component are barely

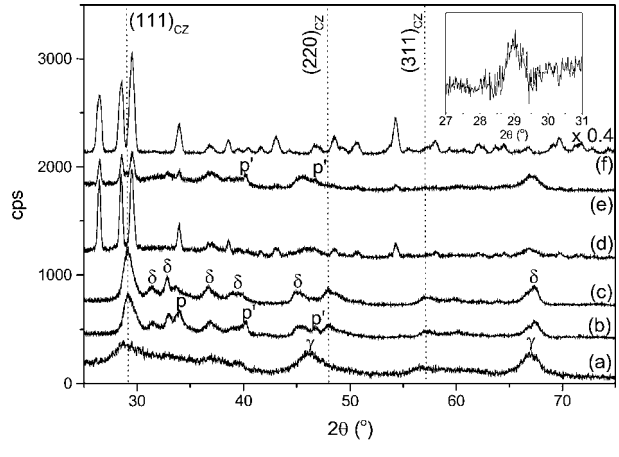

FIG. 1. X-ray diffractograms of (a) fresh PCZ-p, (b) aged PCZ-p, (c) aged CZ, (d) fresh PCZ-m, (e) aged PCZ-m, and (f) the initial cordierite monolith. The inset at the right top shows the pattern obtained by partial subtraction of (d) from (e). CZ subindex refers to the Ce–Zr component. Peaks labeled γ and δ refer to diffractions attributed to γ-Al_2O_3 and δ-Al_2O_3, respectively. For peaks labeled p and p′, see text.

discernible in the pattern of the fresh PCZ-p catalyst (Fig. 1a), for which only a broad, poorly defined peak at ca. 29° can be attributed to the most intense (111) diffraction of that component. In contrast, the most intense peaks of that component are clearly resolved in the diffractogram of the aged PCZ-p system (Fig. 1b), which indicates that a significant degree of sintering of the Ce–Zr mixed oxide is produced as a consequence of the aging treatment. Other changes occurring on aging of PCZ-p affected the alumina component, which is mainly transformed from γ-Al_2O_3 to δ-Al_2O_3, as revealed by comparing the patterns of Figs. 1a and 1b. Careful analysis of the diffraction pattern of the aged PCZ-p catalyst (Fig. 1b) reveals the presence of additional peaks at 33.97° (labelled p), and at 40.25° and 46.76° (labelled p′), which cannot be attributed to other transitional aluminas, by comparison with the pattern of the reference-support CZ aged under similar conditions (Fig. 1c). The positions of peaks p and p′ coincide with those showing appreciable intensity for the thermodynamically most stable phases (17–19) of, respectively, PdO (JCPDS 06-0515) and Pd (JCPDS 01-1201). The presence of these features in the pattern of the aged PCZ-p catalyst indicates that a significant sintering of the Pd component is also produced upon aging. With respect to the catalysts in the form of monoliths (the patterns of which are shown in Figs. 1d and 1e corresponding to fresh and aged PCZ-m catalysts, respectively) the diffractograms are mainly dominated by peaks corresponding to the cordierite support (whose pattern is shown in Fig. 1f), which impedes analysis of those patterns. In any case, a comparative analysis suggests that transformations occurring on aging of the PCZ-m system are similar in nature to those taking place for the PCZ-p catalyst. Thus, palladium sintering is indicated by the presence of peaks p′ in the pattern of the aged PCZ-m system while transformations involving the alumina component appear to occur also, on the basis of slight changes in the peak positions of that component and of the appearance of new peaks in the pattern of the aged system. In this respect, the presence of a peak at ca. 33.0°, which was slightly shifted to a higher angle with respect to peaks observed in that zone for δ-Al_2O_3 (compare Figs. 1c and 1e), suggests that a certain amount of θ-Al_2O_3 (diffractogram JPCDS 47-1771) might also have been produced on aging of the PCZ-m system. On the other hand, sintering of the Ce–Zr mixed oxide component is suggested by the appearance of a peak at ca. 29.0°, revealed by performing subtraction operations between the patterns of Figs. 1e and 1d (as shown in the inset of Fig. 1), in the pattern of the aged PCZ-m catalyst.

Sintering of the Ce–Zr mixed oxide induced by aging treatment of both PCZ-p and PCZ-m is more clearly seen by the analysis of electron diffraction rings (Fig. 2) and in dark-field TEM images of the catalysts (Fig. 3). Thus, while relatively broad and barely discernible peaks of the Ce–Zr mixed oxide are observed in the electron

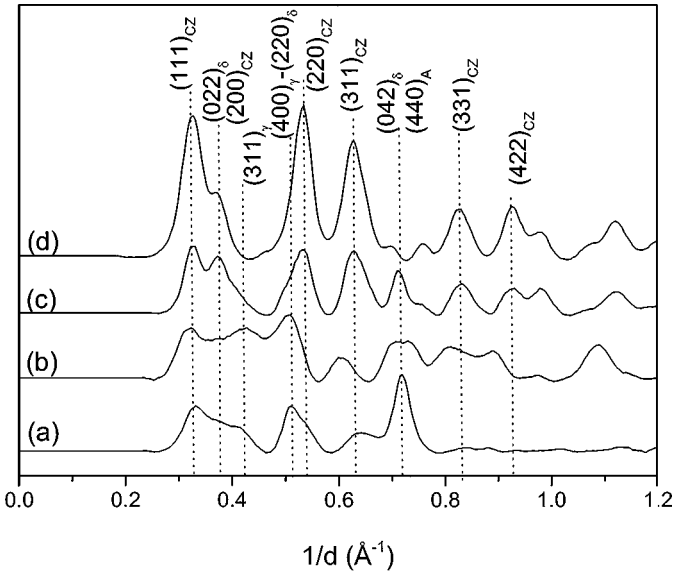

FIG. 2. Radial (angle averaged) densitometry patterns of the electron diffraction rings observed in specific zones of (a) fresh PCZ-p, (b) fresh PCZ-m, (c) aged PCZ-p, and (d) aged PCZ-m. Vertical dotted lines mark the strongest reflections attributed to Ce–Zr mixed oxide and alumina-related phases (subindexed CZ and γ and δ, respectively).

diffraction patterns of the fresh catalysts, a considerable narrowing of those peaks is observed for both systems on aging (Fig. 2). Accordingly, dark-field TEM images of PCZ-m (Fig. 3) show that the Ce–Zr mixed oxide average particle size increases from ca. 3 to 9 nm on aging, while increases from ca. 2 to 10 nm are observed when similar experiments are performed on PCZ-p (results not shown).

With respect to the bulk structural and compositional levels of the Ce–Zr mixed oxide present in each case, the absence of significant splittings in the electron diffraction peaks attributable to this component suggests that pseudocubic mixed oxide phases, most likely phase t″ according to previous work (14, 15), are present in all cases. On the other hand, analysis of lattice parameters from the most intense (111) reflection in both X-ray and electron diffraction patterns yields values of ca. 5.30 and 5.32 Å for the PCZ-p and PCZ-m materials (in both fresh and aged states), which are roughly consistent with expected values (8) for Ce–Zr mixed oxides, with the compositions observed by chemical analysis (see experimental). Consistent with EDS analysis, results show Ce/Zr (atomic ratio) values in the 0.9–1.1 and 1.1–2.0 ranges for the fresh PCZ-p and PCZ-m catalysts, respectively, which are not significantly modified on aging of the systems.

B. Catalytic Properties of the Powder Catalysts

Figure 4 shows the activity profiles for the fresh and aged powdered catalysts during the $CO–O_2–NO–C_3H_6$ reaction. It is interesting that only marginal differences are observed

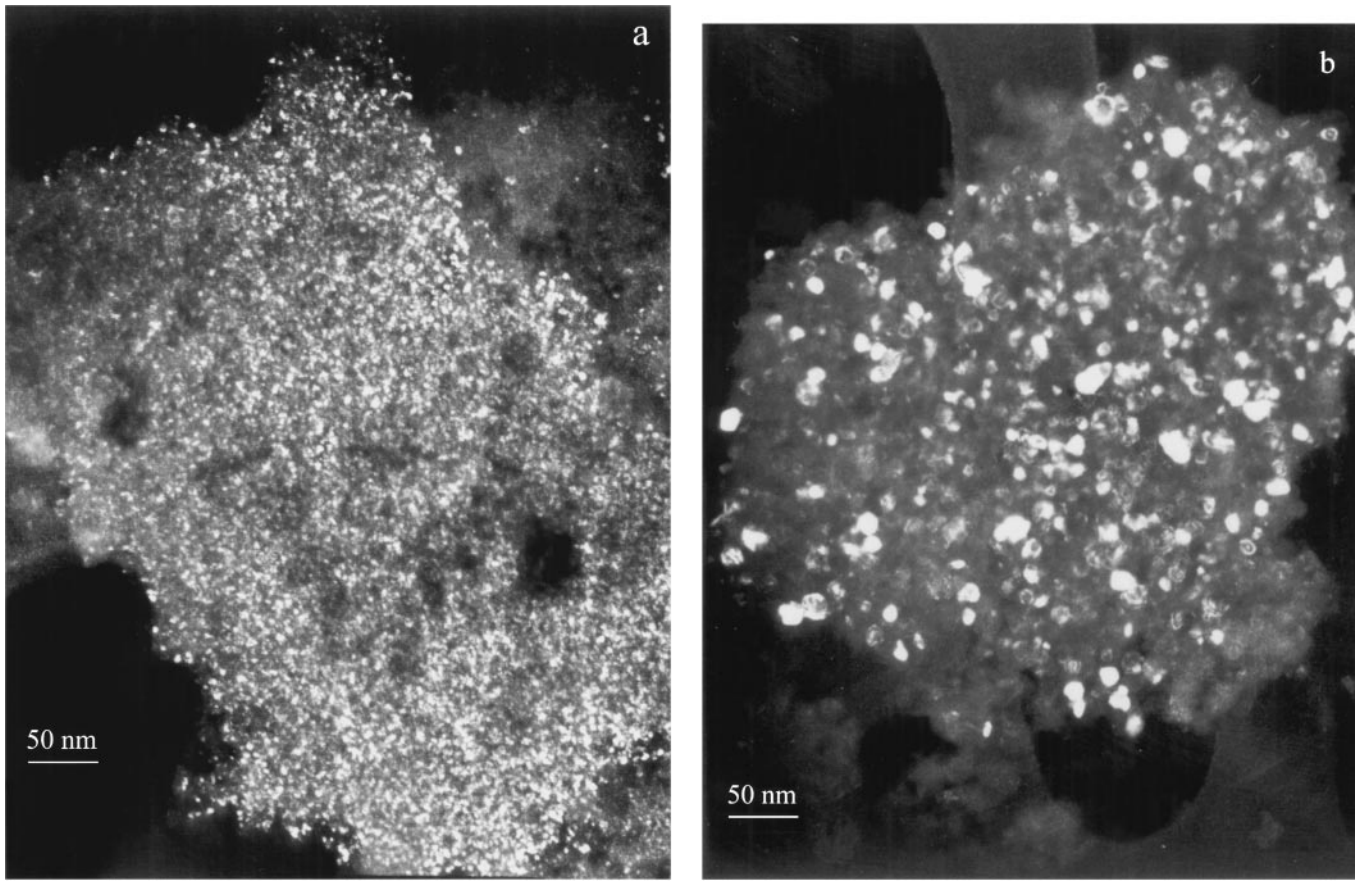

FIG. 3. Dark-field TEM pictures of (a) fresh PCZ-m and (b) aged PCZ-m.

between both catalysts (both in terms of overall conversions of the three pollutants and in terms of N_2 yield—calculated on the basis of mass balance and assuming that adsorption of N-containing molecules is not significant at those conversion temperatures, which roughly follows the NO_x conversion curves), in spite of the significant structural differences detected. Analysis of the conversion profiles shows that the reaction onset is slightly retarded for the aged system although its conversion curve shows a steeper slope, so that only at conversion levels below ca. 50% is the fresh catalyst superior to the aged one. It may be noted that the NO_x conversion below ca. 500 K is affected by adsorption–desorption phenomena on the basis of mass balance, which is consistent with previous temperature-programmed desorption experiments performed on systems of this kind (20). Analysis of results in Table 1 shows that the catalytic behaviour observed with the most complete mixture contrasts with similar experiments performed in the absence of hydrocarbon, which, taking into account the significant sintering of components on going from fresh to aged catalysts, would indicate a generally low degree of structural dependence for the reaction with the most complete mixture. In turn, data in Table 1 show a decreasing activity for CO oxidation, as NO and then C_3H_6 are introduced in the reaction mixture. Similarly, activity for NO reduction also decreases in the presence of hydrocarbon. In a previous paper, the deactivation effects induced by the presence of NO on CO oxidation over this catalyst were analysed in detail (12). In this work, attention is focused mainly on the effects of the presence of the hydrocarbon on the overall performance of the system. It may be noted that earlier work has shown that any of the reactants involved in these reactions can induce poisoning or inhibiting effects on the activity of noble

TABLE 1

Isoconversion Temperatures (K) in Stoichiometric Conditions at 30,000 h^{-1} over Fresh and Aged PCZ-p

	CO			NO_x		HC
	1	2	3	2	3	3
T_{10}	323 (373)	362 (432)	423 (485)	400 (420)	495 (500)	452 (491)
T_{50}	411 (473)	432 (495)	500 (520)	460 (498)	533 (528)	535 (520)
T_{90}	471 (490)	490 (515)	545 (552)	486 (518)	559 (560)	558 (553)

Note. Isoconversion at 10, 50, and 90%. Reactions 1, CO–O_2; 2, CO–O_2–NO; and 3, CO–O_2–NO–C_3H_6. Aged values in parentheses.

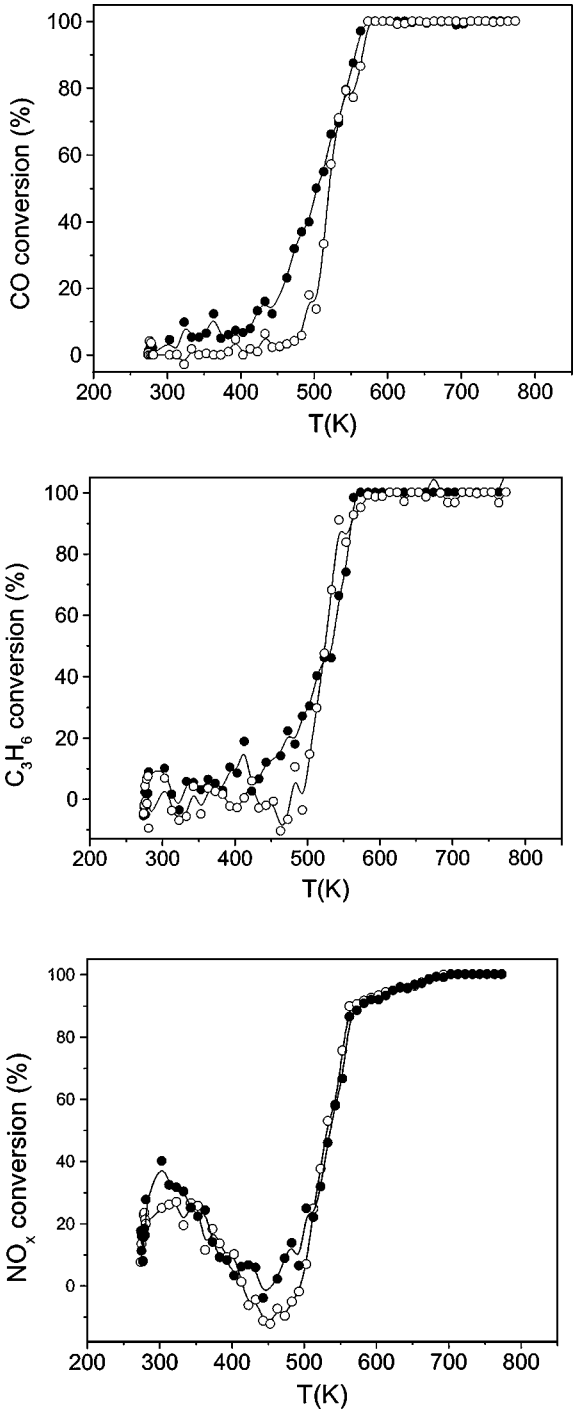

FIG. 4. Conversion profiles for the $CO + O_2 + NO + C_3H_6$ reaction over fresh (filled symbols) and aged (empty symbols) PCZ-p catalysts.

metals for the reduction–oxidation reactions taking place in these systems (21).

DRIFTS spectra obtained under reaction conditions for the fresh catalyst (Fig. 5) show evolution of CO (g) and CO_2 (g), which roughly correlate with the catalytic activity results (Fig. 4). It must be noted that the lower concentrations of NO (g) and C_3H_6 (g) prevent their detection under the same experimental conditions. Only one band at 2159 cm^{-1} appears at relatively low reaction temperatures in the carbonyl-stretching region of the spectra. The origin of this band, which can be assigned to Pd^{2+}-adsorbed carbonyl species, was investigated in detail in a previous contribution (12). These sites are created by NO-induced oxidation of Pd sites at Pd particles in contact with Ce–Zr mixed oxide particles. These are the most active sites for CO oxidation (12, 14). The oxidizing interaction was proposed as that mainly responsible for the lower CO oxidation activity observed for this system in the presence of NO (Table 1). An additional feature was a very weak band at 2246 cm^{-1}, due to NCO species adsorbed on the support (14), which appeared at temperatures from ca. 503 K, in rough agreement with onset of NO reduction. Comparison with experiments in the absence of C_3H_6 (Fig. 6), reveals some characteristics including the hindering effect of propylene on the formation of carbonyls on metallic Pd (bands at 2097–2055 cm^{-1} for on-top species and at ca. 1970 cm^{-1} for bridge carbonyls). This is attributed to strong adsorption of propylene and/or its decomposition fragments onto the metallic particles. Also, a C_3H_6-induced blocking effect of sites at the support or in preventing formation of NCO at the active metal sites is inferred from comparative analysis of adsorbed-NCO species in each case (compare Figs. 5 and 6).

Comparison of other spectral regions with experiments performed under $CO–O_2$ or $CO–O_2–NO$ stoichiometric conditions (results not shown), reveals bands due to the presence of C_3H_6. A band at 1313 cm^{-1} was already apparent following initial contact with the reactant mixture at 303 K, and reached maximum intensity at 403 K. A similar band at 1311 cm^{-1} was reported for the NO/C_3H_6 reaction over Rh/Al_2O_3 (22). Identification of the species responsible for this band is difficult in the absence of other associated bands and with the analysis restricted to wavenumbers above 1200 cm^{-1} (owing to the large absorption of alumina at lower frequencies). It may correspond to the out-of-plane bending mode of a $–CH_3$ fragment (δ_{CH_3}) (23) within a more complex molecular structure for which infrared observation in the transmission mode of other vibration modes is hindered as a consequence of adsorption on metallic Pd particles. Concomitant to the decrease of the band at 1313 cm^{-1}, groups of bands appear at 3001, 2907, 1590, 1392, and 1376 cm^{-1}, showing maximum intensity at ca. 573 K. These bands are characteristic of formate ions adsorbed on alumina, with the two former bands attributed to $\nu_{C–H}$ stretching modes, the bands at 1590 and 1376 cm^{-1} attributed to the asymmetric and symmetric $–COO$ stretching vibrations (ν_{COO} modes), respectively, and the band at 1392 cm^{-1} attributed to the –CH bending vibration (δ_{CH}) (24). Other bands, which appear exclusively in the presence of C_3H_6, are those at ca. 1570 and 1460 cm^{-1}, which are observed to grow from 503 K. These bands can be attributed to

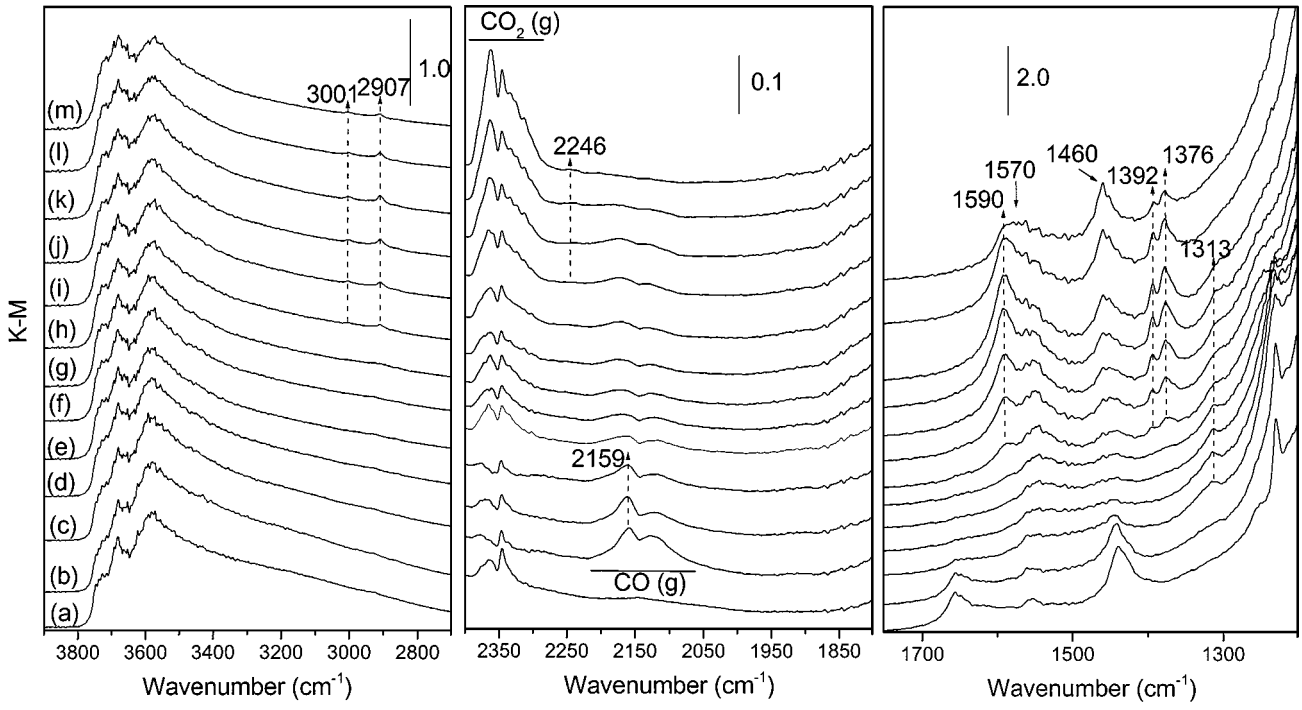

FIG. 5. *In situ* DRIFTS spectra of the fresh PCZ-p sample in a flow of 1% CO, 0.9% O_2, 0.1% NO, and 0.1% C_3H_6, N_2 balance. (a) Before introduction of the reactant mixture. Under reaction conditions at (b) 303, (c) 348, (d) 378, (e) 408, (f) 423, (g) 453, (h) 483, (i) 503, (j) 523, (k) 553, (l) 608, and (m) 653 K. Ordinate axis in Kubelka–Munk units.

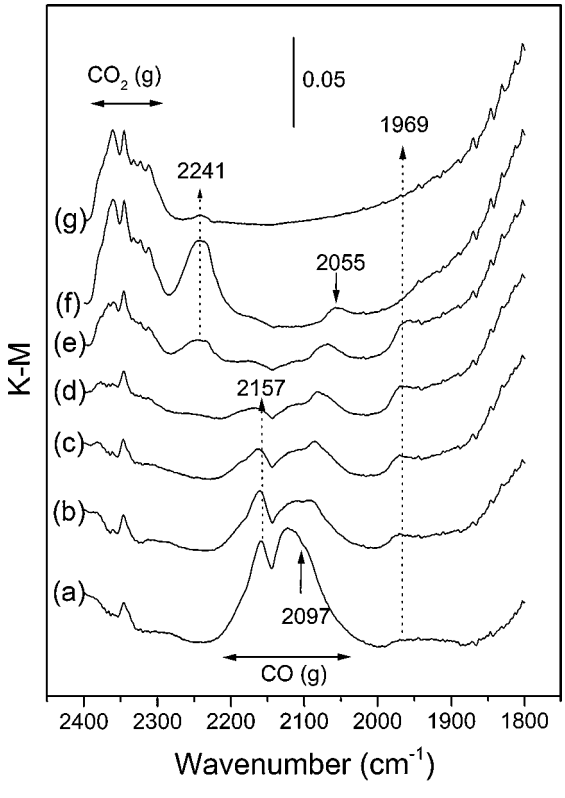

FIG. 6. *In situ* DRIFTS spectra of the fresh PCZ-p sample in a flow of 1% CO, 0.45% O_2, 0.1% NO, N_2 balance, at (a) 303, (b) 363, (c) 393, (d) 423, (e) 453, (f) 483, and (g) 513 K.

adsorbed acetate or acrylate species on the support on the basis of experiments of acetic acid and acrolein adsorption on alumina, which shows exclusively bands of this kind due to ν_{COO} vibrations of the carboxylate group in that complex (22). Observation of acetate species at higher temperatures is consistent with a previous work showing their higher resistance toward decomposition in comparison to adsorbed formate species (25). There are other bands which appear at similar frequencies, as observed when working under CO–O_2 or CO–O_2–NO stoichiometric conditions, such as those at 1545 and 1440 cm^{-1}, which can accordingly be attributed to the ν_{COO} modes of alumina-adsorbed carboxylate species, and which apparently grow until ca. 553 K. Additionally, bands due to hydrogen–carbonate species adsorbed on alumina (bands at 1657, 1439, and 1229 cm^{-1}) are present in the initial sample, their evolution evidencing the rapid decomposition of these species by interaction with the reactant mixture.

The DRIFTS spectra obtained under the same conditions for the aged catalyst (Fig. 7) are essentially similar to those observed for the fresh catalyst, except that a generally lower intensity of bands due to adsorbed species was observed, as a result of the lower surface area of this system. A great similarity is observed between both systems with respect to the stability of the species giving the 1313 cm^{-1} band, although it appears that its maximum intensity (reflecting the temperature at which these species begin to decompose or desorb) is produced at a slightly lower temperature for the

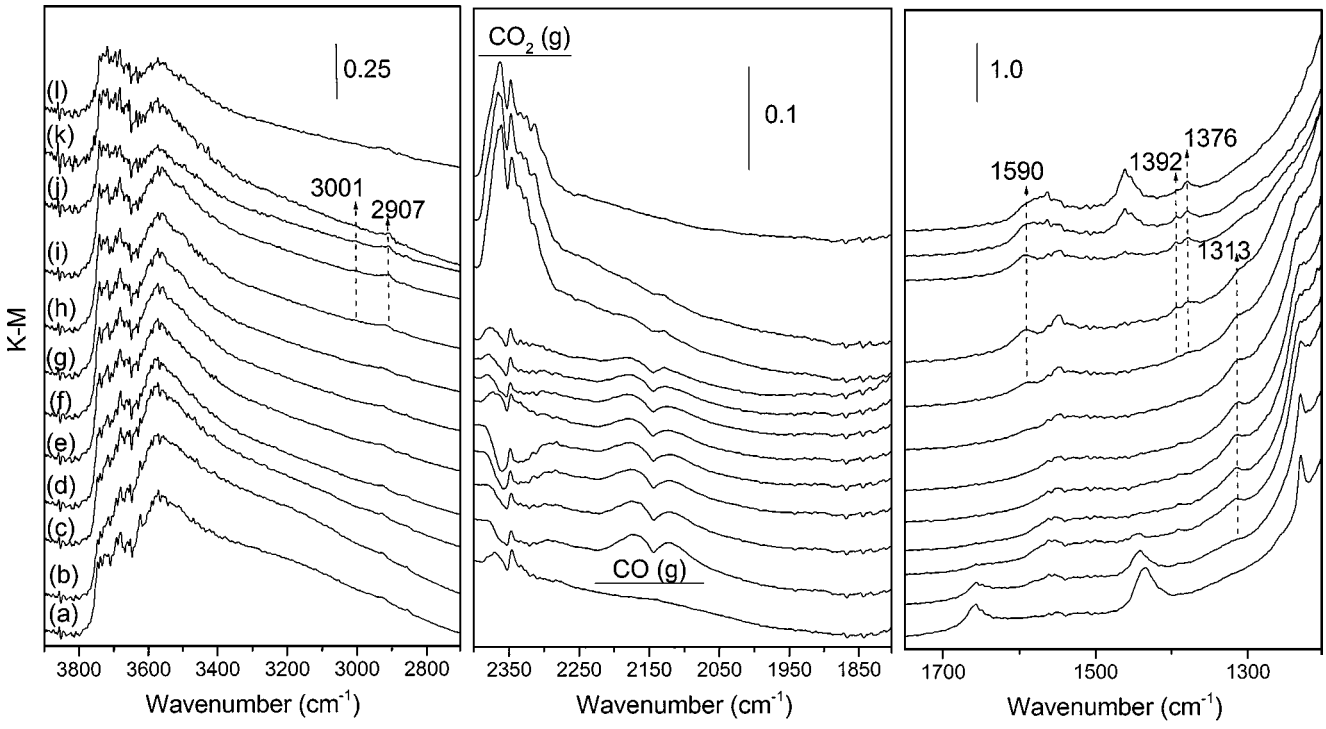

FIG. 7. *In situ* DRIFTS spectra of the aged PCZ-p sample in a flow of 1% CO, 0.9% O_2, 0.1% NO, and 0.1% C_3H_6, N_2 balance. (a) Before introduction of the reactant mixture. Under reaction conditions at (b) 303, (c) 348, (d) 378, (e) 408, (f) 423, (g) 453, (h) 483, (i) 503, (j) 533, (k) 558, and (l) 648 K.

fresh (ca. 408 K) than for the aged (ca. 423 K) sample. Associated with this, the appearance of adsorbed formate bands appears to be produced at somewhat higher temperatures for the aged catalyst than for the fresh one.

Following completed runs under reaction conditions, the samples were cooled under inert gas flow, CO (3% in N_2) was flown at RT, and finally CO (g) was flushed with N_2, and the DRIFTS spectra in Fig. 8 were obtained. The fresh sample shows evidence for mainly metallic Pd (bands for CO on top at 2088 cm^{-1} and bridging species at 1971 cm^{-1}), with a lower intensity of carbonyls adsorbed on partially oxidised Pd particles (band at 2130 cm^{-1}) also being observed (12, 14, 26). In the case of the aged catalyst, a significantly lower intensity of Pd-related carbonyls is observed, in correlation with the sintering of palladium produced on aging. The spectrum of this sample shows mainly the presence of bridging carbonyls adsorbed on metallic Pd particles (band at 1979 cm^{-1}), with a lesser contribution of carbonyls adsorbed on partially oxidised Pd particles (band at 2130 cm^{-1}) (12, 26). These experiments indicate the presence of mainly metallic Pd particles in the post reaction condition of the catalysts. The differences in the relative ratios between the intensities of on-top and bridging carbonyls, when comparing fresh and aged states of the catalyst in these experiments, would suggest changes in the particle morphology induced by the aging treatment.

On the basis of these results and considering also the onset temperatures of the reactions (Fig. 4), the light-off performance for elimination of the three pollutants must

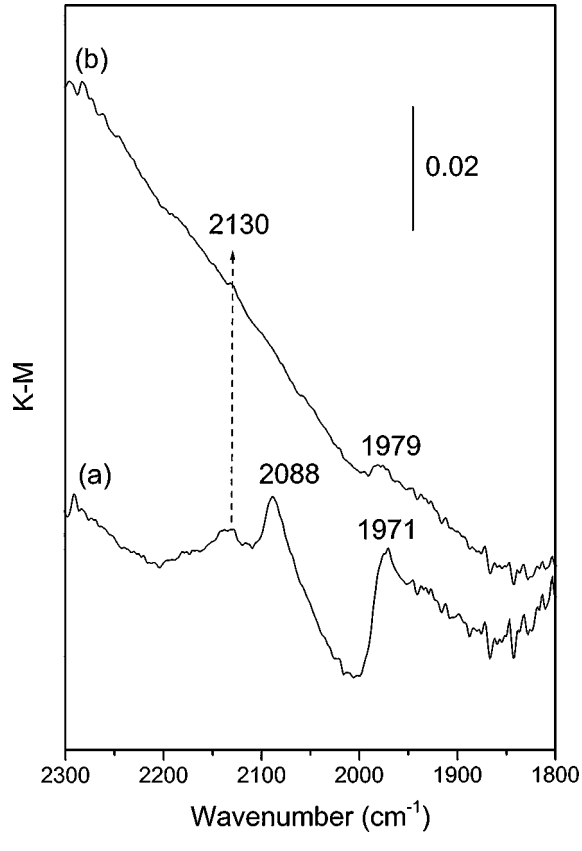

FIG. 8. DRIFTS spectra after CO admission at RT and flushing with N_2 on used PCZ-p. (a) Fresh and (b) aged specimens.

mainly be limited by a self-poisoning effect due to the presence of fragments derived from C_3H_6 adsorption, which form molecular complexes possessing at least $-CH_3$ moieties (giving rise to the band at 1313 cm^{-1}). The relatively strong adsorption of these fragments at the temperatures at which CO and NO react in the absence of C_3H_6 (see Table 1) indicates that activation of CO and NO is retarded as a consequence of their hindered adsorption on the Pd metallic surface. As soon as those C_3H_6-derived fragments evolve from the metal and/or metal-support interface, as a consequence of processes involving probably their complete oxidation and/or spillover to the support as partially oxidised intermediates (giving rise mainly to formate and acetate species), free catalytically active sites appear (most likely located at Pd–$Ce_xZr_{1-x}O_2$ interfaces, according to previous works (12, 15)). Note that the temperature at which the 1311 cm^{-1} band begins to diminish (423 K) coincides with the upper temperature limit where the ethylidine species obtained from adsorption of propene on metal surfaces are dehydrogenated to leave C_xH_y species (27), thus accounting for the loss of bands due to CH_3 groups. These sites released for adsorption of CO and NO are created at the surface of the metallic particles the molecules being rapidly oxidised and reduced, since the temperatures at which this process occurs is sufficiently high (according to data in Table 1) for activation of these molecules to occur. Certain similarities can be found to exist between this reaction scheme and recent proposals based on studies of the catalytic performances of Pt/Al_2O_3 catalysts for a similar reaction (28). In the same context, the large similarities in the performances of fresh and aged PCZ-p in the presence of C_3H_6 must be attributed to the relatively low structural sensitivity observed for the proposed propene self-poisoning effect, as suggested by the *in situ* DRIFTS results (Figs. 5 and 7).

C. Engine Tests

Figures 9 and 10 show the essential characteristics of the raw emission produced by the engine in the conditions employed. Figure 9 shows the temperature and λ value evolutions during the test. The λ value was calculated according to the formula (1, 6)

$$\lambda = \{1 + 0.02545([CO] + [H_2] + 10[THC] - 2[O_2] - [NO_x])\}^{-1},$$

in which it is assumed that $[CO]/[H_2] = 3$ (1) and the concentrations are expressed as volume percent (of C_3 for THC). As under practical conditions, the test starts with the catalyst under air having a large λ value, which rapidly decreases, showing a slight oscillation at the beginning, with a minimum at $\lambda = 0.95$ after 34 s and a maximum at $\lambda = 1.09$ after 107 s. Then, as shown in more detail at the bottom of Fig. 9, the λ value decreases gradually until a value of $\lambda = 1.003$ ($T = 723$ K) is achieved at the end of the test. Characteristic points in this curve are the following: $\lambda = 1.020$, $T = 575$ K; $\lambda = 1.010$, $T = 603$ K; and $\lambda = 1.005$, $T = 669$ K. It is important to note that the exhaust condition is essentially lean throughout the test, although the oxidant character of the gas mixture is progressively decreased. Figure 10 shows the raw emission concentrations for the three main pollutants. In the three cases, a maximum is produced at the beginning of the test, with stationary values of 0.41%, 435 ppm, and 180 ppm being observed for CO, THC, and NO_x, respectively, at the end of the test.

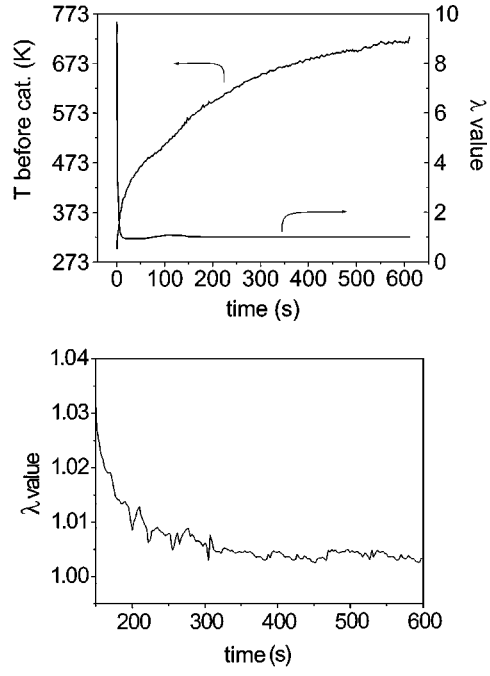

FIG. 9. Characteristics of the raw emission in the engine system under conditions specified in the experimental part. (Top) Temperature and λ evolutions; (bottom) detail of λ evolution.

Figure 11 shows the conversion profiles for the three main pollutants. In this case, practically no differences are observed over the whole conversion range between the fresh and aged PCZ-m catalysts for any of the pollutants. T_{50} isoconversion values were observed at ca. 563 K and 543 K for CO and THC, respectively, while NO_x reduction started at around 623 K, with ca. 40% conversion being achieved at the end of the test ($T = 723$ K). The poor performance of the catalysts for NO_x conversion is probably a consequence of the lean condition of the exhaust gas, as inferred from analysis of the combined activity profiles (Fig. 11), since it is known that significant difficulties for TWCs exist, particularly for Pd-only catalysts (4, 14), for NO_x reduction under those conditions (1, 3). This is supported by the fact that only a slightly higher NO_x reduction performance (X_{NO_x} = ca. 45% at 723 K) has been observed over a reference commercial (Pt–Rh) TWC evaluated under the

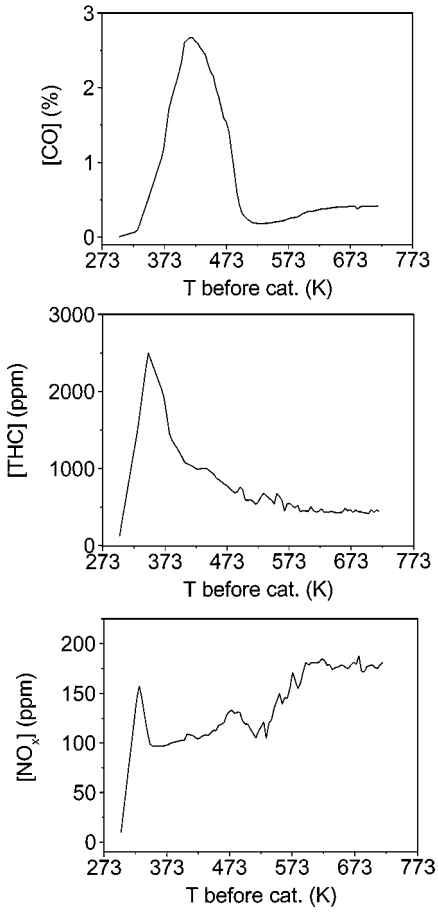

FIG. 10. Characteristics of the raw emission in the engine system under the conditions specified in the experimental part. (Top) CO emission; (middle) total hydrocarbons emission; (bottom) NO_x emission. Concentrations in vol%, vol ppm C_3, and vol ppm NO_x ($NO + NO_2$), respectively.

same conditions, while the performances of this commercial catalyst for CO and HC oxidation were essentially similar to those obtained for PCZ-m. As shown in Fig. 11, both THC and NO_x are removed to a certain extent at temperatures below reaction onset, which must be due to adsorption–desorption processes on the basis of mass balance and which are usually observed to occur, particularly when working at relatively low space velocity and in the presence of ceria-related promoters (20), at those temperatures (7).

Similar phenomena as those proposed for the PCZ-p catalysts, involving self-poisoning effects by hydrocarbons, can be invoked to explain the similar performances observed for fresh and aged PCZ-m systems. The closer similarity of both systems observed in the engine tests, with respect to laboratory tests on powdered catalysts, can be attributed to the considerably higher rate of reaction-temperature increase produced in the engine system (Fig. 9). Differences between catalytic activity results observed for the powder and monolithic systems in this study must be a consequence of the different nature of the reaction system in each case in terms of factors such as the nature of the reactants (a more complex HC mixture being present for the engine test), the relative shift of the reaction mixture from the stoichiometric condition, or the presence of composition oscillations for the engine system. Obviously, lesser differences between the components constituting the catalyst in each case are probably also relevant in this respect. These factors may explain the slightly higher temperatures required for onset of CO and HC oxidation in the engine tests with respect to the model gas

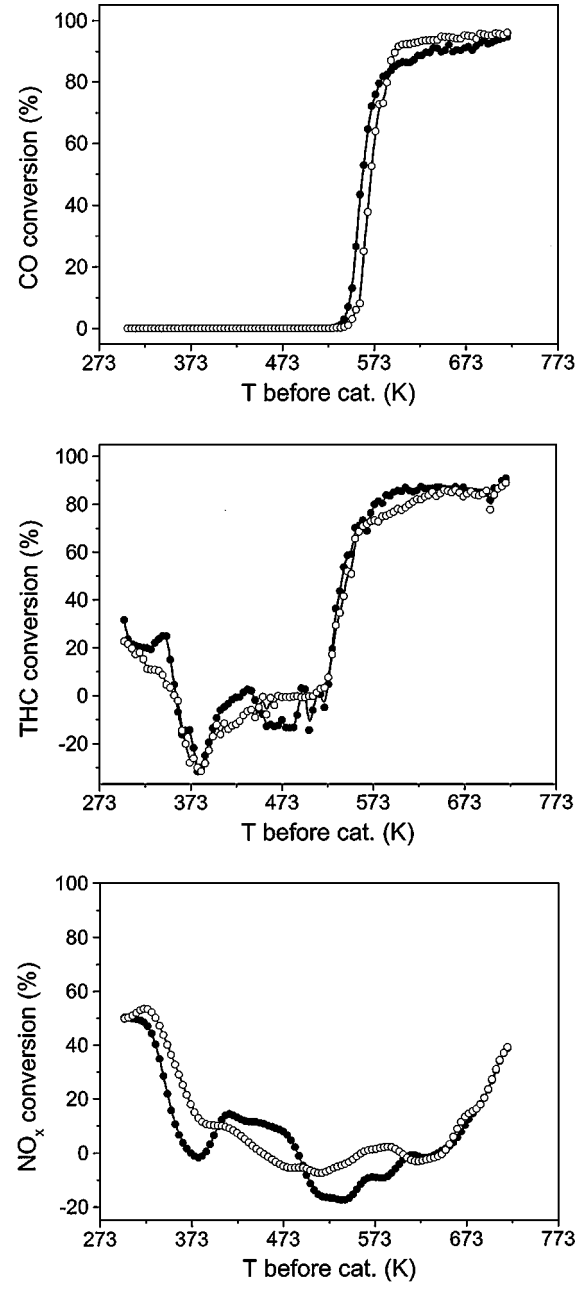

FIG. 11. Conversion profiles for the reaction in the engine system over fresh (solid symbols) and aged (open symbols) PCZ-m catalysts.

tests, as well as the fact that in the engine tests, HCs apparently begin to burn before CO oxidation onset (in contrast to the model gas tests), showing a somewhat irregular and relatively slow conversion behaviour. In any case, the results obtained for both catalytic systems, and most particularly for the tests obtained under real conditions with the engine system, indicate the relative unimportance of structural changes induced by thermal treatments (at least up to the degradation point achieved for the catalysts used in this study on aging and also considering the relatively low space velocities employed) when the reaction mixture contains HC (as under practical conditions). This also justifies efforts leading to more efficient management of the HC component, such as employment of HC traps or optimised engine operation to obtain richer mixtures in the cold-start stream (7), or noble metal promotion with alkaline metals (28). A further point to remark on, which may also help to explain the comparatively good performance of the aged systems, is the fact that the PCZ systems used in this work contain Ce–Zr mixed oxide phases which show fairly good structural stability after aging at 1273 K, although, certainly, further experiments on more deteriorated systems would be required to corroborate this point.

CONCLUSIONS

The consequences of thermal degradation by oven-aging of $Pd/Ce_xZr_{1-x}O_2/Al_2O_3$-related three-way catalysts, which leads to significant sintering of Pd and Ce–Zr mixed oxide active components, are relatively insignificant in terms of their light-off performances when tested either with synthetic gas mixtures in laboratory tests (powdered catalysts) or under engine emissions (catalysts in the form of monoliths). This is attributed to the presence of HCs in the reaction mixture which, following HC decomposition on the catalytically active sites, act as catalytic poisons by the relatively strong adsorption of fragments. The desorption of these fragments show little structural sensitivity. This has been confirmed for the powdered samples by *in situ* DRIFTS, which show the presence of complexes containing $-CH_3$ fragments adsorbed on the metallic Pd particles at the temperatures at which both CO and NO are activated in the absence of C_3H_6.

ACKNOWLEDGMENTS

We thank Prof. J. A. Cairns (Dundee) for access to the engine test facility and Dr. M. Brogan (Johnson Matthey) for supplying the cordierite monoliths used in this study. A. M.-A., A. B. H. and A. I.-J. thank the Comunidad de Madrid for grants under which this work has been carried out and for financial assistance (A. M.-A. and A. I.-J) under the "Ayudas para estancias breves en centros de investigación extranjeros" program. Financial help by CICYT (project MAT2000-1467) is also acknowledged.

REFERENCES

1. Lox, E. S. J., and Engler, B. H., *in* "Environmental Catalysis" (G. Ertl, H. Knözinger, and J. Weitkamp, Eds.), p. 1. Wiley-VCH, Weinheim, 1999.
2. Trovarelli, A., *Catal. Rev. Sci. Eng.* **38**, 97 (1996), and references therein.
3. Hu, Z., Wan, C. Z., Lui, Y. K., Dettling, J., and Steger, J. J., *Catal. Today* **30**, 83 (1996).
4. Skoglundh, M., Johansson, H., Löwendahl, L., Jansson, K., Dahl, L., and Hirschauer, B., *Appl. Catal. B* **7**, 299 (1996).
5. van Yperen, R., Lindner, D., Mubmann, L., Lox, E. S., and Kreuzer, T., *Stud. Surf. Sci. Catal.* **116**, 51 (1998).
6. González-Velasco, J. R., Botas, J. A., Ferret, R., and González-Ortiz, M. A., *Stud. Surf. Sci. Catal.* **116**, 73 (1998).
7. Lafyatis, D. S., Ansell, G. S., Bennett, S. C., Frost, J. C., Millington, P. J., Rajaram, R. R., Walker, A. P., and Ballinger, T. H., *Appl. Catal. B* **18**, 123 (1998).
8. Kašpar, J., Fornasiero, P., and Graziani, M., *Catal. Today* **50**, 351 (1999).
9. Jiang, J. C., Pan, X. Q., Graham, G. W., McCabe, R. W., and Schwank, J., *Catal. Lett.* **53**, 37 (1998).
10. Ozaki, T., Masui, T., Machida, K., Adachi, G., Sakata, T., and Mori, H., *Chem. Mater.* **12**, 643 (2000).
11. Di Monte, R., Fornasiero, P., Kašpar, J., Graziani, Gatica, J. M., Bernal, S., and Gómez-Herrero, A., *Chem. Commun.* 2167 (2000).
12. Martínez-Arias, A., Fernández-García, M., Iglesias-Juez, A., Hungría, A. B., Anderson, J. A., Conesa, J. C., and Soria, J., *Appl. Catal. B* **31**, 51 (2001).
13. Yao, M. H., Blaird, N. J., and Kunz, F. W., *J. Catal.* **166**, 67 (1997).
14. Fernández-García, M., Martínez-Arias, A., Iglesias-Juez, A., Belver, C., Hungría, A. B., Conesa, J. C., and Soria, J., *J. Catal.* **194**, 385 (2000).
15. Fernández-García, M., Martínez-Arias, A., Iglesias-Juez, A., Hungría, A. B., Anderson, J. A., Conesa, J. C., and Soria, J., *Appl. Catal. B* **31**, 39 (2001).
16. Martínez-Arias, A., Fernández-García, M., Ballesteros, V., Salamanca, L. N., Otero, C., Conesa, J. C., and Soria, J., *Langmuir* **15**, 4796 (1999).
17. Niu, C.-M., Rieger, P. H., Dwight, K., and Wold, A., *J. Solid State Chem.* **86**, 175 (1990).
18. Graham, G. W., Jen, H.-W., McCabe, R. W., Straccia, A. M., and Haack, L. P., *Catal. Lett.* **67**, 99 (2000).
19. Kepinski, L., and Wolcyrz, M., *Appl. Catal. A* **150**, 197 (1997).
20. Cataluña, R., Arcoya, A., Seoane, X. L., Martínez-Arias, A., Coronado, J. M., Conesa, J. C., Soria, J., and Petrov, L. A., *Stud. Surf. Sci. Catal.* **96**, 215 (1995).
21. Wei, J., *Adv. Catal.* **24**, 57 (1975).
22. Anderson, J. A., and Rochester, C. H., *J. Chem. Soc. Faraday Trans. 1* **85**, 1117 (1989).
23. Zaera, F., *Langmuir* **12**, 88 (1996).
24. Busca, G., Lamotte, J., Lavalley, J. C., and Lorenzelli, V., *J. Am. Chem. Soc.* **109**, 5197 (1987).
25. Captain, D. K., and Amiridis, M. D., *J. Catal.* **184**, 377 (1999).
26. Xu, X., and Goodman, D. W., *J. Phys. Chem.* **97**, 7711 (1993).
27. Koestner, R. J., van Hove, M. A., and Somorjai, G. A., *CHEMTECH* **13**, 376 (1983).
28. Konsolakis, M., Macleod, N., Isaac, J., Yentekakis, I. V., and Lambert, R. M., *J. Catal.* **193**, 330 (2000).